Task 4: Improvements to marine PBL in WRF

AQRP Project 24-021

Improving WRF representation of coastal, marine, and residual boundary layers and quantifying the effects on ozone prediction

Prepared by

Yuxuan Wang, University of Houston

James Flynn, University of Houston

March 15, 2025

1. Introduction

The project aims at validating and improving marine planetary boundary layer (PBL) predictions over Galveston Bay (the Bay) and the Gulf of America (the Gulf) by the Weather Research and Forecasting (WRF) model using the abundance of offshore observation data from Tracking Aerosol Convection ExpeRiment-Air Quality (TRACER-AQ) studies during July – October 2021 (TAQ1) (Jensen et al., 2021), April – October 2022 (TAQ2, TCEQ), and the 2023 Mobile and Offshore Air Quality Monitoring Project during May-Oct 2023 (TAQ3, TCEQ). In proceeding with Task 3, it was found that the WRF v4.6.0 base model has consistent gaps in simulating marine boundary layer height and its diurnal cycles. Over the Bay, the planetary boundary layer height (PBLH) exhibits a strong diurnal cycle, with the model underestimating PBLH in the afternoon. Over the Gulf, both observed and simulated PBLH show a less distinct diurnal variation than the Bay, with the model overestimating PBLH during the morning and underestimating it during the afternoon. The performance of the WRF model was also found to be location- and time-dependent, varying across different locations such as the Houston Ship Channel (HSC) or areas near land versus those farther away. These findings highlight the fact that PBL-related parameterizations and assumptions in WRF need improvements and tuning to better match observations over water bodies around Houston/Galveston.

In Task 4, we conducted the model perturbation simulations by adjusting the physics ensembles in the WRF v4.6.0 base model. We identified the key physics parameters and their ranges that most likely affect the evolution of PBLH in the Mellor-Yamada-Nakanishi-Niino Level 2.5 (MYNN2) scheme, along with some other additional parameters like surface roughness and albedo in the model. In addition to the physics perturbations, we also conducted numerous sensitivity simulations by implementing different cumulus schemes and urban physics schemes, which are found effective in improving the PBLH from the base simulations. We evaluated the perturbation simulations by using the numerous onshore and offshore datasets from different field campaigns in the Houston-Galveston-Brazoria (HGB) region including the Bay and the Gulf. The evaluation of these simulations helped to identify the most sensitive physics parameters with their corresponding values, which are effective at producing the PBLH values closer to the observations.

2. Base model configuration and performance

The Weather Research and Forecasting (WRF) model version 4.6.0 with the Advanced Research WRF (ARW) solver was employed to simulate meteorological fields for three domains (**Figure 1)** over the contiguous United States (d01 - 12km×12km), Southeast Texas (d02 - 4km ×4km), and the Houston-Galveston region (d03 - 1.33km×1.33km), respectively. All three domains have identical vertical resolutions with 30 vertical levels from the surface to ~100 hPa. As the base WRF configurations, we used the local closure Mellor-Yamada-Nakanishi-Niino Level 2.5

(MYNN2) PBL scheme (Nakanishi & Niino, 2009a), Morrison double moment (2M) microphysics scheme (Morrison et al., 2009), Rapid Radiative Transfer Model (RRTMG) longwave and shortwave radiation schemes (Iacono et al., 2008), Monin-Obukhov similarity surface layer scheme (Chen et al., 1997), Noah land-surface module (Chen & Dudhia, 2001), and the New Tiedtke cumulus parameterization (Tiedtke, 1989; Zhang et al., 2011). The initial and boundary conditions (IC/BC) for domain d01 were derived from the High-Resolution Rapid Refresh (HRRR) model, while the IC/BC for d02 were generated from d01, and those for d03 were generated from d02. These configurations were selected from our previous work that yielded the best prediction of overall meteorological conditions during the TAQ1 field campaign period (X. Liu et al., 2023).

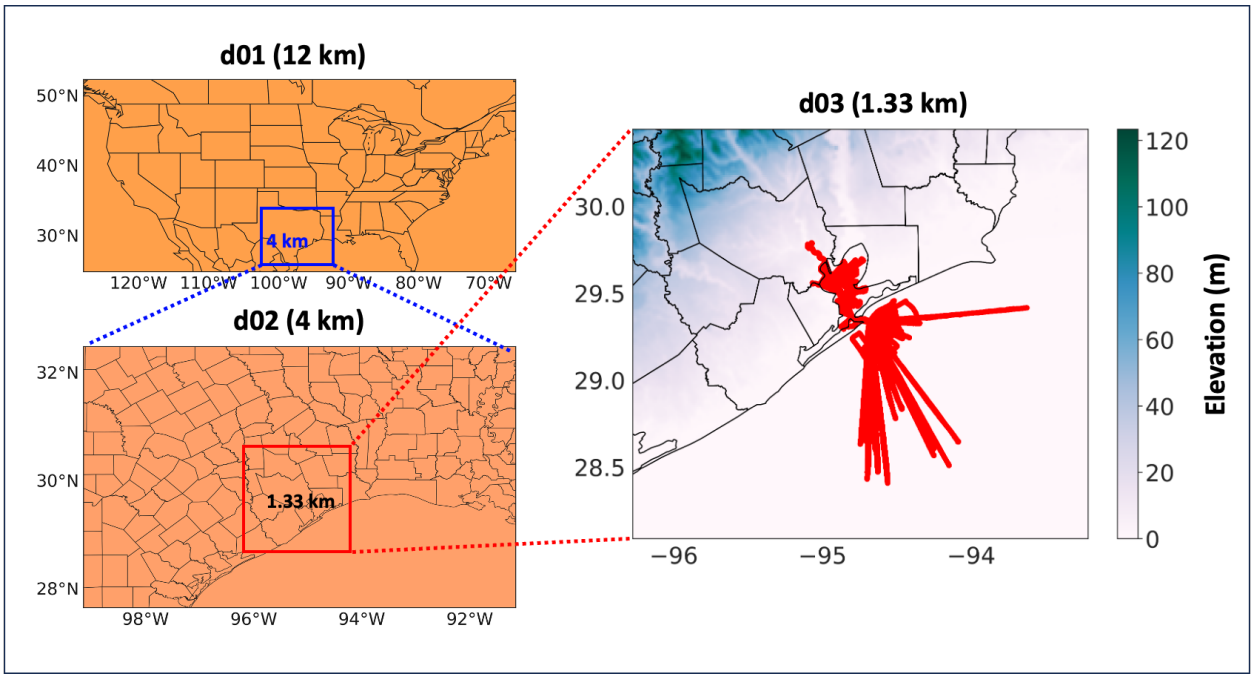

Figure 1 WRF domains showing d01 (contiguous United States), d02 (Southeast Texas), and d03 (Houston-Galveston) regions. Red lines in d03 are the locations of ship-based measurements for the selected months.

The Task 3 Report discussed the limitations of the base model's performance in simulating the marine PBL and its diurnal variations. In addition to those limitations, the base simulation of WRF was found to present the 'cloud-like' patterns in the PBLH distribution over the waters under certain conditions (**Figure 2**). The cloud-like features are caused by a sharp change in PBLH within neighboring grids, which is deemed unrealistic. Upon further investigation, we attributed this artifact to model limitations in simulating wind speed and direction under small-scale cyclonic conditions, which causes sudden updrafts and/or downdrafts of air parcels, leading

to the observed cloud-like patterns in PBLH. This finding indicates that offshore PBLH prediction in WRF is affected by the choice of cumulus schemes. For example, after we replaced the New Tiedtke Cumulus scheme used in baseline configurations with the New Simplified Arakawa-Schubert (NSAS) scheme, the unrealistic patterns in the PBLH distribution over the Gulf are not present (**Figure 2b**). Drawing from this exercise, we added different cumulus schemes as part of the sensitivity simulations to be carried out in Task 4, and the related results are described in this report.

We discovered another issue of PBLH with the baseline configuration in the urban region. The model shows persistent higher PBLH over urban Houston during nighttime (**Figure 3a**). The PBLH hotspots over urban Houston exhibit a fixed boundary which is unrealistic and appears due to the simplified treatment of urban land types in the model. One consequence of this PBLH artifact is that it causes the model prediction of nitrogen oxides (NOx) to be unrealistically low over urban Houston during nighttime hours and thus it is of importance for the overall model performance. We found the issue could be resolved by implementing a more advanced scheme for treating urban areas, such as the Urban Canopy Model (UCM) and Building Effect Parametrization (BEP). For example, after adopting the UCM scheme in the simulations (**Figure 3b**), the high PBLH hotspots over the urban Houston area are mitigated. We note the intriguing effect that UCM leads to changes in PBLH over the water despite it being implemented only in the urban region. It is probably because it affects the land-sea thermal gradient by changing the heat and moisture budgets in urban Houston. Seeing this effect, we added UCM as part of the sensitivity simulations to be carried out in Task 4, and the related results are described in this report.

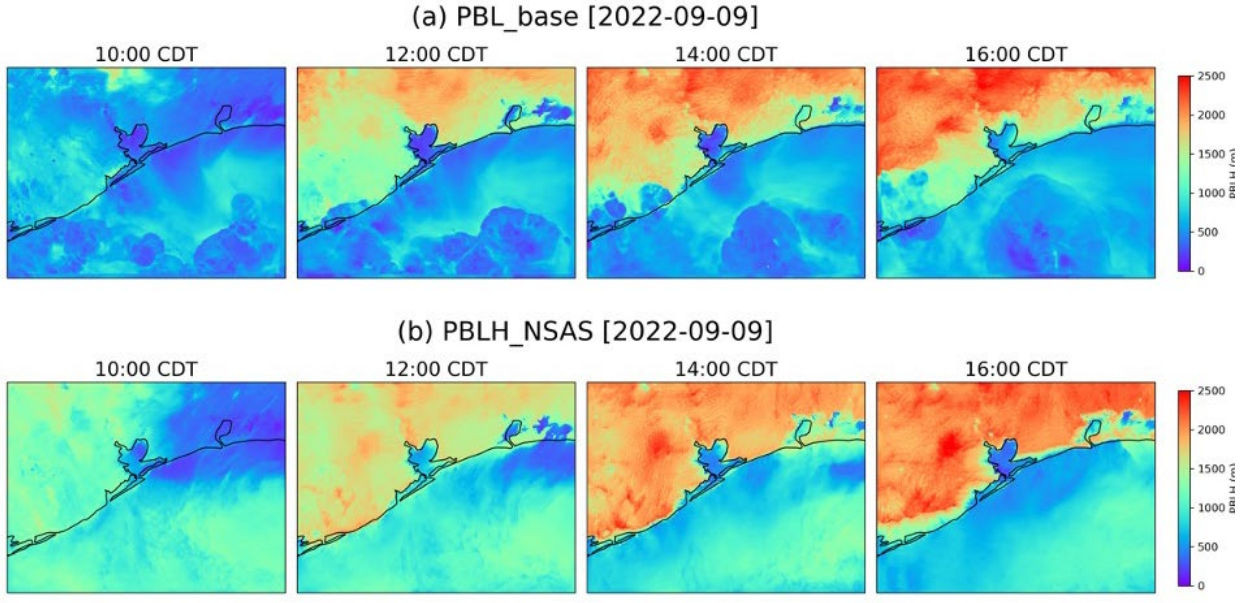

Figure 2 Spatial distribution of hourly PBLH (m) variation from (a) the base simulation and (b) base simulation with New Simplified Arakawa-Schubert (NSAS) cumulus scheme

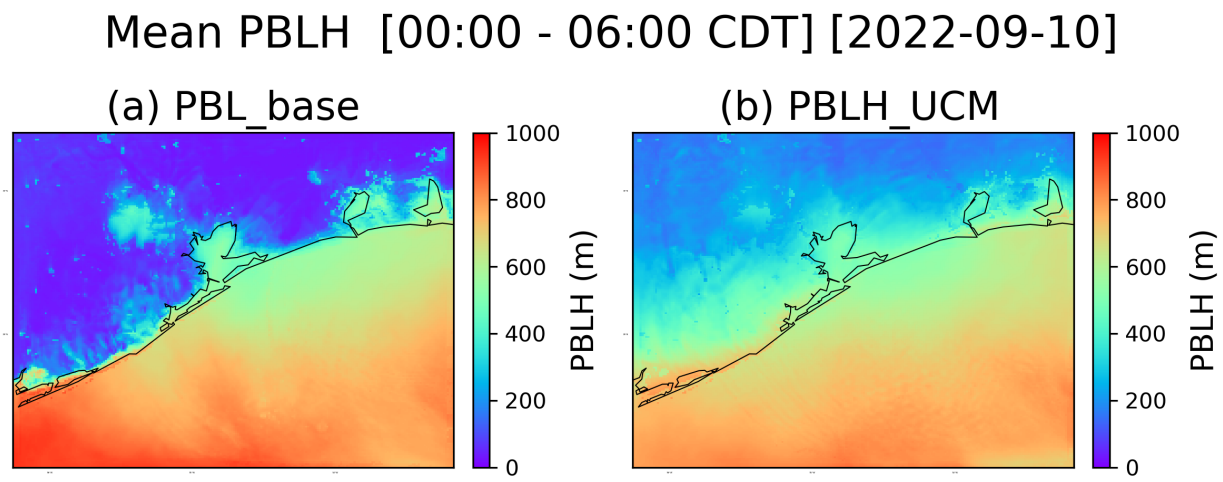

Figure 3 Spatial distribution of Night-time (00:00 – 06:00) mean PBLH from (a) the base simulation (b) the base simulation with Urban Canopy Model (UCM).

3. Selection of physics parameters and schemes

3.1. Physics Parameters

WRF incorporates various schemes to simulate the evolution and development of the PBL. The sensitivity of these schemes depends on the topographical and environmental conditions, making it essential to identify the most effective schemes for the region. Our previous study (Liu et al., 2023) evaluated different PBL schemes over the diverse onshore and offshore environments of Houston-Galveston-Brazoria (HGB) region including the Bay and the Gulf as sampled by the TAQ1 campaign. The MYNN with 2.5 closure (MYNN2) scheme was identified as the best choice for the region among all available PBL schemes in WRF with the least bias compared to PBLH observations from the TAQ1 campaign. The evaluation of WRF PBL with different field campaign observations, conducted in Task 3 of the present project, indicates that the model underestimates the afternoon PBLH over the water and fails to capture the diurnal cycle accurately. To address this gap, we identified key parameters and constants adopted in MYNN PBL scheme that are likely to impact the PBLH, as shown in **Table 1**. The Table includes the values of the parameters used in the base model and their possible ranges reported from the literature that can be used to fine-tune the model predictions.

Table 1 Physics parameters identified for perturbation in MYNN PBL scheme

Parameters /Constants	Description	Default Values	Perturbation Range	References
B1	Constant for Dissipation Rates	24	[12,36]	Nakanishi & Niino, (2009)
B2	Constant for Dissipation Rates	15	[7.5, 22.5]	Nakanishi & Niino, (2009)
α1	Constant for Turbulent length scale (L_T)	0.23	[0.2-0.3]	(Yang et al. 2017)
Pr	Turbulent Prandtl Number	0.74	[0.7 – 2.0]	(Pithan et al., 2015)
Z0	Surface roughness	0.0185	[0.01 – 0.03]	(Yang et al. 2017)
C3	Closure Constant	0.33	[0.33 – 0.5]	(Huang & Peng, 2017)
ALBD	Albedo	0.08	[0.6-0.9]	(Liu et al., 2022)

The MYNN PBL scheme is a turbulence closure model with several constants and unknown parameters that represent physical factors such as the dissipation rates of total kinetic energy (TKE), pressure co-variances, and turbulence fluxes, which are determined empirically. TKE dissipation rates measure turbulence strength and are proportional to the energy transfer from larger to smaller eddies. These rates are parameterized as a function of the mixing length (L) and the closure constants B1 and B2. Higher values of B1 and B2 result in lower TKE dissipation rates, which is expected to increase the PBLH (Yang et al., 2017). The default values of B1 and B2, along with their ranges, are detailed in Table 1.

The mixing length (L) typically determines the distance an air parcel with energy can travel before dispersing, and it is expressed as the harmonic sum of L_s, L_T, and L_B. L_s represents the length scale determining mixing near the surface, while L_B is effective for the stable boundary layer (Nakanishi & Niino, 2009). L_T dominates the mixing length in the middle to upper convective boundary layer. Our primary goal is to improve the model PBLH mostly during unstable cases, so we choose to perturb L_T, which depends on the value of α1. Thus, we perturbed α1 for a range of values to test its sensitivity to PBL.

Turbulent Prandtl number (Pr) is the ratio of diffusivity of momentum to that of heat. The values for Pr range from 0.74 to 2. The choice of Pr determines the near-surface gradients of temperature and humidity. Lower values of turbulent Prandtl number lead to warmer convective boundary layers, especially in tropical and sub-tropical regions (Pithan et al., 2015). We expect the choice of Pr to be sensitive in the coastal regions where the convective boundary layer is usually seen during the daytime.

The closure constant (C3) represents the effects of shear and buoyancy in the MYNN2 scheme whose values are theoretically determined to be 0.33 for isotropic turbulence and 0.5 for the convective boundary layer (Nakanishi & Niino, 2009). The default value for the base case is 0.34, which is subject to subsequent perturbations of 0.42 and 0.5.

Roughness length (Z0) is a surface-dependent parameter that typically refers to the maximum height at which winds diminish to zero due to surface friction. This term is related to the transfer of heat, momentum, and moisture and is parameterized in surface schemes. Due to unresolved sea wave effects, roughness length may have higher uncertainties in coastal areas. An improved representation of roughness length can affect wind speed near the surface, leading to increased turbulence and, consequently, a rise in PBL.

3.2. WRF configuration test

In addition to perturbing physical parameters described above, we conducted sensitivity simulations by selecting different cloud and urban physics schemes aimed to mitigate the unrealistic 'cloud-like' features of PBL (**Figure 2**) and PBL hotspots in urban Houston (**Figure 3**) from the baseline simulations. To resolve the former, a single-layer urban canopy model (UCM) was implemented in WRF which considers the momentum drag effects of buildings and the energy exchange between the urban structure and the atmosphere. UCMs are expected to better predict the PBLH over urban areas. To resolve the cloud-like features in the spatial distribution of PBL, we replaced the New Tiedtke cumulus scheme with the NSAS scheme. Furthermore, we tested the MYNN3 scheme, which is more advanced as it employs a prognostic approach to diagnose sub-grid scale vertical motions, rather than a diagnostic one in MYNN2. **Table 2** lists these additional sensitivity simulations conducted so far.

Table 2 Additional schemes adopted for the sensitivity runs

Schemes	**Description**	**Default Settings**	**Customized Settings**
MYNN	PBL scheme	2.5	3.0
UCM	Urban Canopy Model	off	on
Cumulus physics	Switched to different schemes	New Tiedtke	New Simplified Arakawa-Schubert (NSAS)

3.3. Selected days for model perturbation

The selected days for the model perturbation are based on the model evaluation in Task 3, as well as our previous modeling analysis of TAQ1 and TAQ2 campaign datasets. A total of 9 days were chosen for model perturbation/sensitivity simulations: July 27-28, September 9, and

September 24-26, 2021; September 8-10, 2022; and May 19 and September 9-10, 2023. The selection criteria for these dates consider multiple factors, including various locations in the Bay and the Gulf, both near and far from land, including the Houston Ship Channel (HSC). Other criteria include different times of day, varying pollutant levels, and the availability of both mobile and stationary observational data. These diverse factors help ensure a comprehensive evaluation of the model. **Figure 4** shows the locations for each selected day with the time-of-day for each observation point.

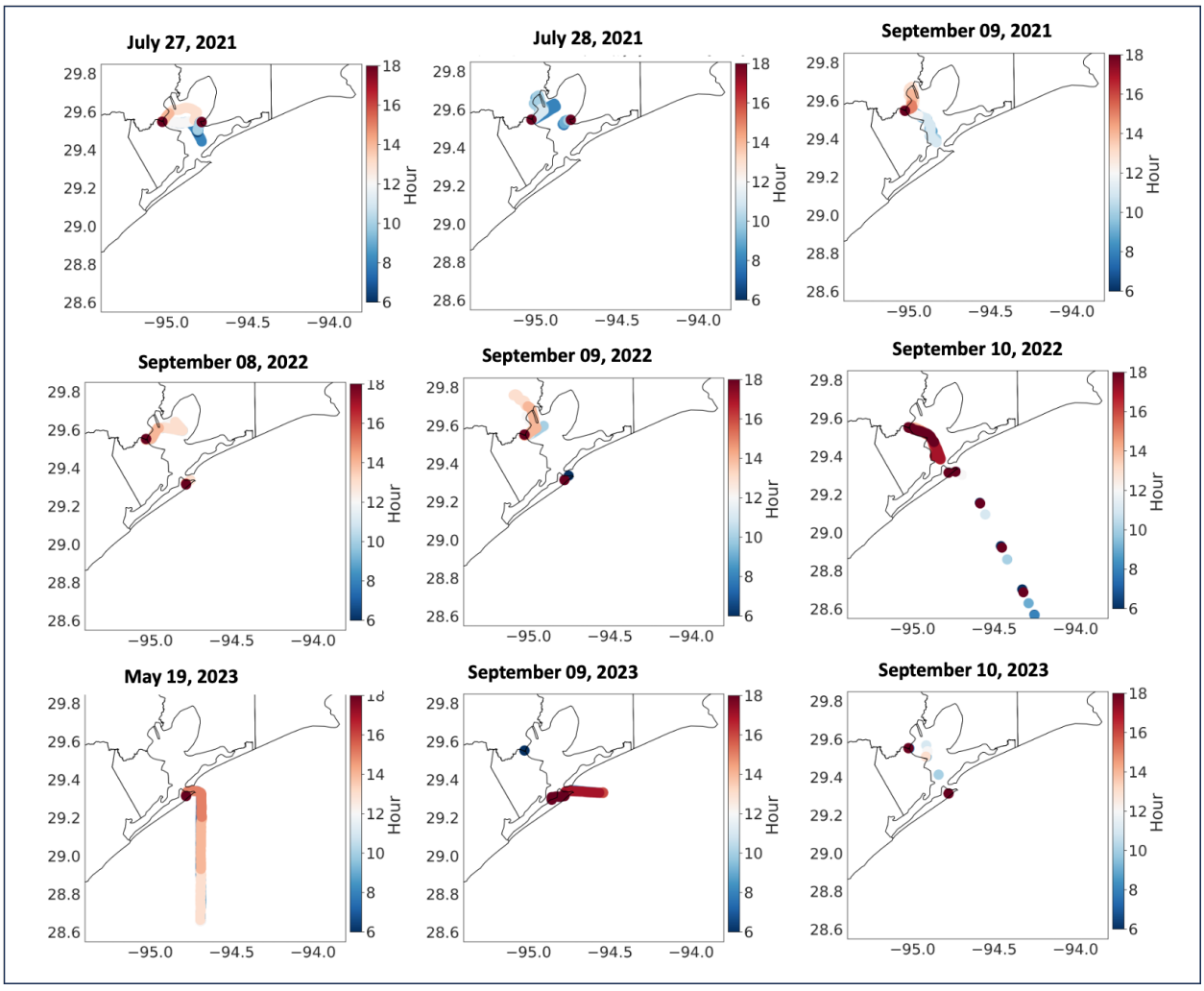

Figure 4 Location of the selected days for model perturbation. Color in the spatial map represents the time of observation.

4. Perturbation simulations and results

4.1. Experimental Setup for model perturbation

Table 3 lists all the model perturbations conducted so far. Each simulation was conducted for all the selected days listed in Section 3.3, resulting in more than 200 simulation-days. The first group of simulations (PBLH1 – PBLH10) are designed to test the sensitivity of identified physics parameters across a range of values. The aim is to identify optimal parameters that improve the model's ability to simulate marine PBL and its diurnal variation. The second group of simulations (PBLH11-21) tested various cumulus schemes and urban physics schemes, along with their potential combinations, to resolve issues seen in the base simulations described above.

Table 3 Different set of simulations designed by perturbing the physics parameters and changing the schemes.

Simulation ID	**PBL Scheme**	**Cumulus Physics Scheme**	**Urban Physics Scheme**	**Parameter Perturbation**
PBL_base	MYNN2.5	New Tiedtke	off	None
PBLH1	MYNN2.5	New Tiedtke	off	B1 = 36, B2 = 22.5
PBLH2	MYNN2.5	New Tiedtke	off	B1 = 30, B2 = 18.5
PBLH3	MYNN2.5	New Tiedtke	off	$\alpha 1 = 0.27$
PBLH4	MYNN2.5	New Tiedtke	off	$\alpha 1 = 0.50$
PBLH5	MYNN2.5	New Tiedtke	off	C3 = 0.50
PBLH6	MYNN2.5	New Tiedtke	off	C3 = 0.42
PBLH7	MYNN2.5	New Tiedtke	off	Pr = 2
PBLH8	MYNN2.5	New Tiedtke	off	Pr = 1.37
PBLH9	MYNN2.5	New Tiedtke	off	Z0 = 0.02 (for water)
PBLH10	MYNN2.5	New Tiedtke	off	albedo = 0.09
PBLH11	MYNN3.0	New Tiedtke	off	MYNN 2.5 to MYNN3.0
PBLH12	MYNN2.5	NSAS	off	New Tiedtke to NSAS
PBLH13	MYNN2.5	New Tiedtke	On	UCM
PBLH14	MYNN2.5	NSAS	On	NSAS+UCM
PBLH15	MYNN2.5	NSAS	on	NSAS+UCM+PBLH5
PBLH16	YSU	New Tiedtke	on	UCM
PBLH17	BouLac	New Tiedtke	on	UCM
PBLH18	YSU	New Tiedtke	on	BEP scheme
PBLH19	BouLac	New Tiedtke	on	BEP scheme
PBLH20	YSU	New Tiedtke	on	BEM scheme
PBLH21	BouLac	New Tiedtke	on	BEM scheme

4.2. PBLH changes from model perturbations compared to observations

Each of the perturbed PBLH results obtained from more than 200 simulation days was compared to the base simulations and with onshore and offshore observations from TAQ1, TAQ2, and TAQ3. The impact of the perturbations is not consistent throughout the domain or the selected days. Some of them have a significant impact on PBLH over the land with small changes over the water, while others degraded PBL over land despite improving it over the water. After conducting a thorough analysis, we selected a few of the simulations that increased PBLH over the water with less impact on land and are performing better on most of the selected days. The four best simulations identified are PBLH4, PBLH5, PBLH12, and PBLH14. PBLH4 refers to the simulations for the perturbed value of $\alpha 1$. PBLH5 refers to the perturbed value of closure constant C3. PBLH12 refers to the simulations that implement newer cumulus schemes called NSAS. PBLH14 includes a combination of the UCM with the NSAS cumulus scheme. The details of their simulation setups are listed in **Table 3**.

After selecting those four simulations, we conducted a combined simulation between PBLH5 and PBHL14 as a test case. While this experiment improved the PBLH over water, it decreased PBLH significantly over the land, which contradicted with land-based PBL observations and hence not desirable.

Figure 5 compares the frequency distribution of daytime (08:00 – 18:00 CDT) PBLH between the observations, the base simulation, and the chosen perturbations (PBLH4, PBLH5, PBLH12, and PBLH14) for all the selected days combined. The comparison is shown separately for the Bay (**Figure 5**a) and the Gulf (**Figure 5**b). In the Bay, observed PBLH shows two distinct peaks, the first one corresponding to the increased PBLH shortly after sunrise and the second one mostly during the afternoon. In all the model experiments, the first peak is skewed towards the higher values than in the observations, meaning the model persistently overestimates the morning rise of PBLH in the Bay. The second peak is of more interest because it predominantly occurs in the afternoon when photochemistry is most active. The base simulation misses this peak by underestimating afternoon PBLH. PBLH12 and PBLH14 closely replicate the second peak, indicating they improve upon the base simulation by predicting higher afternoon PBLH in the Bay that matches better with the observations.

In the Gulf, the PBLH simulated by all the perturbation runs is primarily concentrated around the lower values. This is the same as the base simulation, indicating a fundamental difficulty of the model in reproducing the higher PBL occasions in the Gulf. PBLH12 has a longer tail toward the higher values than other simulations, making it the closest to the observations. PBLH4 is comparable to PBLH5 in the Gulf, although it performed relatively poorly over the Bay. Based on the frequency distribution evaluation, we focused on PBLH5, PBLH12, and PBLH14 in the

subsequent sections and conducted additional diagnostic evaluations on them to understand the impact of the perturbations from those simulations.

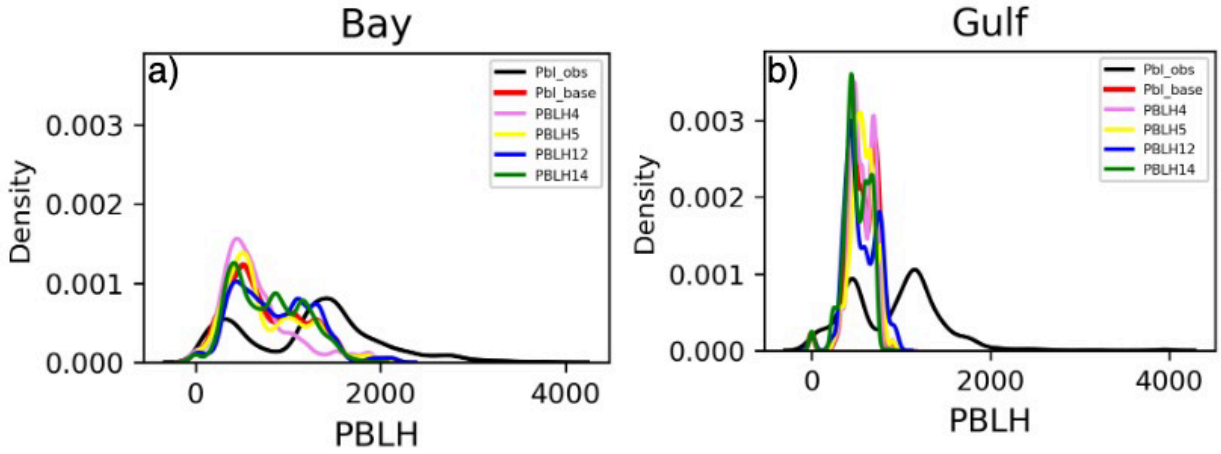

Figure 5 Frequency distribution of daytime (08:00 - 18:00 CDT) PBLH for all the selected days over the a) the Bay and b) the Gulf

Figure 6 shows the spatial variability of the ceilometer-observed PBLH compared to the base simulation, along with the differences between the perturbed and base simulations for the three selected best simulations (PBLH5, PBLH12, and PBLH14) over Galveston Bay and the Gulf. The spatial variation shown in Figure 5 covers only the selected days (July 27-28 and September 9, 2021; September 8-10, 2022; and May 19 and September 9-10, 2023) for the model perturbations. Across all the selected days through the three years, the base model consistently underestimates the PBLH for both the Bay and Gulf.

For most of the Bay, compared to the base simulation, all three selected perturbation simulations show an increase in PBLH. PBLH variations in the observed data, base simulation, and perturbed model simulations are different across the years and locations in the Bay. This could be due to the influence of differences in observation time and location. For example, in 2021, in the northwest of the Bay, the boat was mobile mostly in the afternoon. During this time, PBLH increased by ~300 m in PBLH12 compared to the base simulation, while it increased by ~200 m in PBLH5. PBLH14 showed a slight decrease. By contrast, in the northeast Bay, the boat was mobile mostly in the morning, and the base simulation slightly overestimated the PBLH. All the perturbation simulations performed better compared to the base simulation with closer values to the observation. In the morning, PBLH14 performed better, while in the afternoon PBLH5 and PBLH12 performed better.

Across the three years, the ceilometer observed PBLH in 2022 is much higher compared to 2021 and 2023. In 2022, the base simulation highly underestimates the PBLH over the Bay. The perturbed simulations reduced the underestimation with PBLH values getting closer to the observed values. Among the three perturbed simulations, for example around the HSC, PBLH12 and PBLH14 show an increase of ~200 m compared to the base simulation, while PBLH5 does not show any increase. Towards the northeast of the Bay, both PBLH12 and PBLH14 show an increase of ~400 m. PBLH5 also shows an increase in PBLH over the northeast part of the Bay but with a slightly smaller increase than PBLH12 and PBLH14. In 2023, the base simulation slightly underestimated the PBLH in and around the south HSC, where the boat was mostly mobile. PBLH12 simulation shows an increase in PBLH compared to the base, whereas PBLH5 and PBLH14 show little change compared to the base simulation.

The ceilometer-observed PBLH is lower over the Gulf compared to the Bay. The base model performed better in capturing PBLH variations for the Gulf compared to the Bay. Over the Gulf, in 2022, the observations were mostly from the eastern part of the Gulf, except when the boat was docked. The ceilometer-observed PBLH in these regions ranged around ~1000 m, and the base simulation slightly underestimated these PBLH values. Compared to the base, all three perturbation simulations show an increase in PBLH, with the best performance from PBLH12. In 2023, in and around the northeast part of the Gulf (closer to the Bay), the ceilometer-observed PBLH shows slightly higher values than the southern part of the Gulf (towards the large open water bodies). The base simulation for both of these regions underestimated the PBLH. PBLH5 shows a subtle increase in PBLH compared to the base for the northeast Gulf but PBLH12 and PBLH14 slightly decreased the PBLH. Over the southern part of the Gulf, all three-perturbation simulations show a subtle increment in PBLH, getting closer to the observation.

In summary, when ceilometer-observed PBLH is high over the water, all three of the selected perturbation simulations provide better PBLH estimates than the base model. However, when the observed PBLH values are low, mostly over the Gulf, the perturbation simulations show little difference compared to the base model. Overall, over the water in the morning, PBLH14 performed better in predicting the PBLH, while in the afternoon PBLH12 performed better. PBLH12 refers to the simulations that implement newer cumulus schemes called NSAS. PBLH14 includes a combination of the UCM with the NSAS cumulus scheme.

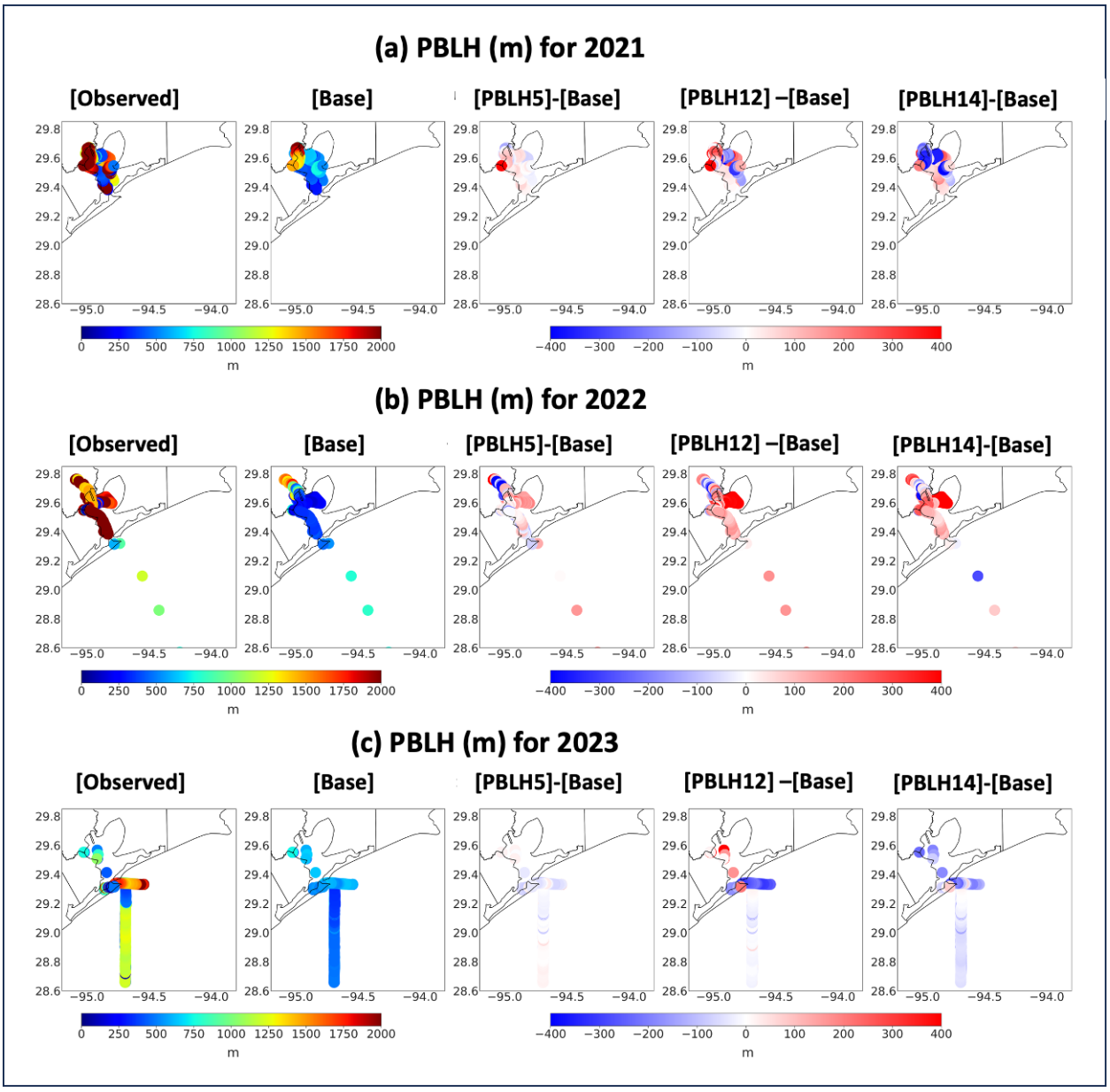

Figure 6 Spatial variation of observed, WRF [Base], [PBLH5] minus [Base], PBLH12 minus [Base], and PBLH14 minus [Base] PBLH (m) for the selected days (a) July 27-28 and September 09, 2021, (b) September 8-10, 2022, and (c) September 9-10, 2023, for the Bay.

4.3. Temporal and spatial changes in PBLH from model perturbations

After establishing that the selected perturbation models better match the observations over the offshore regions for the selected days, we further analyzed the modeled spatial and temporal variations of PBLH over land, the Bay, and the Gulf. For this analysis, we focused on September

in 2021, 2022, and 2023 due to abundant observations in September compared to other months and used all available observations from each September to compare with the selected perturbation experiments. In addition to the ground-based observations, we also used airborne High Spectral Resolution Lidar 2 (HSRL-2) mixing layer height data from September 2021, which covered a broad region, to compare with the model PBLH.

Given that PBL has distinct diurnal cycles, we first examined the changes in the hourly spatial variation of PBLH from the selected perturbation simulations, in comparison to the base and observation data. There is one common day, September 9, from the selected days in each of the three years. This day was used as an example to reveal the spatial and temporal effects of the perturbation experiments. **Figure 7** shows the hourly (9:00, 12:00, and 15:00 CDT) spatial distribution of PBLH from the base simulation and the three selected perturbation experiments (PBLH5, PBLH12, and PBLH14) by taking their differences from the base. The ceilometer observed PBLH is overlaid as filled circles in the base plot. The circles include the stationary observation from the LaPorte and Battleground sites (median values for the selected hour) and mobile observations from the different boats and MAQL1 which are overlaid at the sampling time without averaging. The spatial variation plot shows that the effect of the perturbation is not homogeneous across the region or over the years. For example, on September 9, 2021 (**Figure 7**a) at 9:00 CDT in the morning, the perturbation simulation PBLH12 and PBLH14 shows an increase in PBLH of ~100 m over the Bay and PBLH5 shows an increase of ~50 m compared to the base simulation, getting closer to the ceilometer observed PBLH. During noon time, the base model underestimates the PBLH over the Bay and slightly overestimates at the LaPorte. Compared to the base, all three perturbed simulations show an increase of PBLH (~200 m) over the Bay and a decrease at LaPorte, improving upon the base. In the afternoon, at 15:00 CDT, the base model again shows an underestimation of PBLH over both the Bay and LaPorte. Compared to the base, PBLH5 and PBLH12 show an increase of PBLH over both locations while PBLH14 only shows an increase of PBLH over the Bay but not at LaPorte. This suggests that the perturbed simulation improved the PBLH estimation over both the water and surrounding land close to the water for September 2021 with a better improvement from PBLH12.

For 2022 and 2023, the hourly spatial variation of PBLH in the Base simulation shows unrealistic ‘cloud-like’ patterns, with a sharp change in PBLH within neighboring grids. As discussed in Section 2, these patterns were influenced by the choice of cumulus schemes used in the model. When the New Tiedtke Cumulus scheme used in the baseline configurations is replaced with the NSAS scheme in PBLH12 and PBLH14, the unrealistic patterns in the PBLH distribution are resolved. When comparing the PBLH from the base simulation with the perturbed simulations for both 2022 and 2023, an increase in PBLH is observed in the perturbed simulations (Figure 6b & 6c), mostly in regions where a sharp decrease in PBLH occurs in the base simulation.

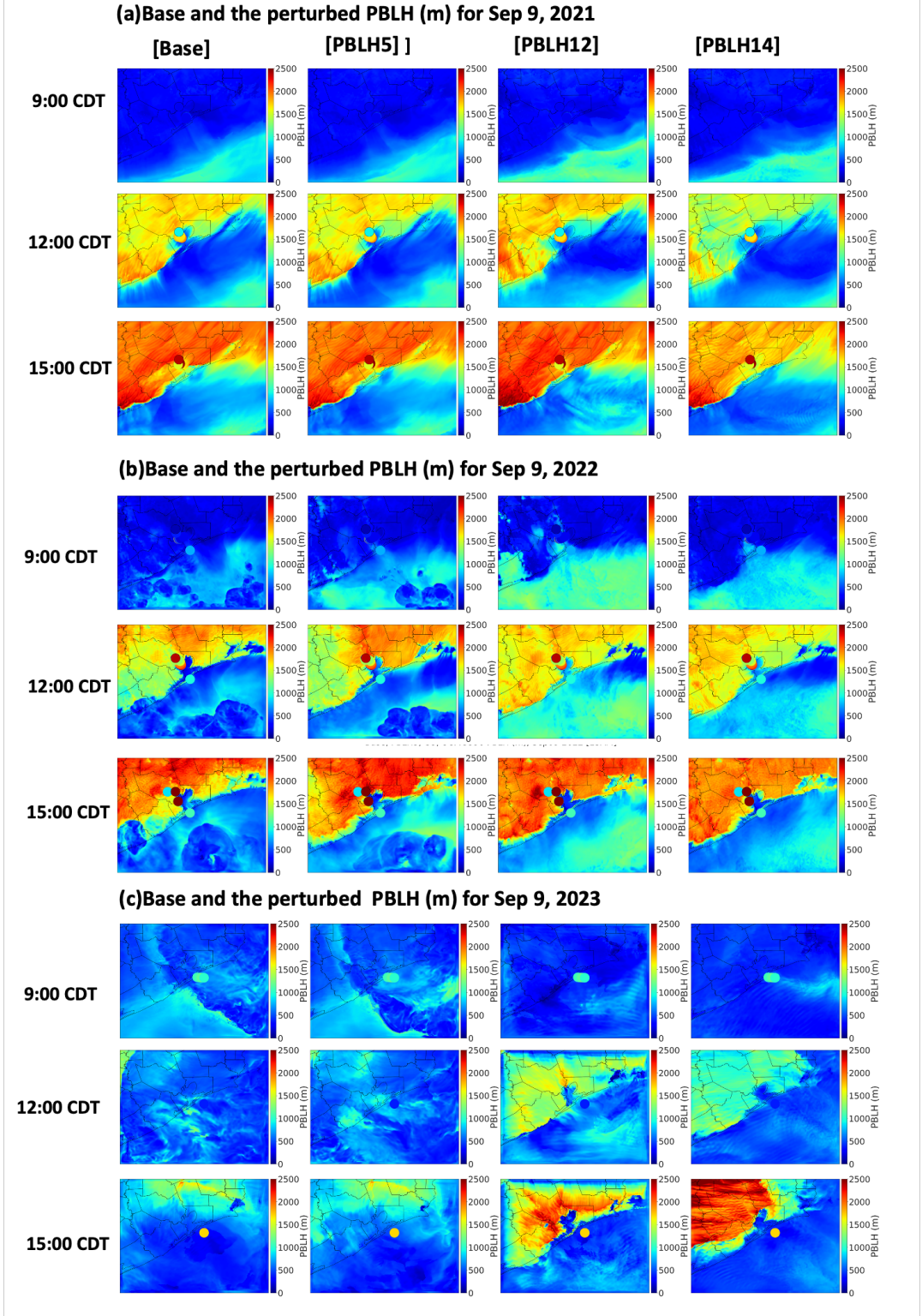
(a)Base and the perturbed PBLH (m) for Sep 9, 2021
[Base]
[PBLH5]]
[PBLH12]
[PBLH14]
9:00 CDT
12:00 CDT
15:00 CDT
(b)Base and the perturbed PBLH (m) for Sep 9, 2022
9:00 CDT
12:00 CDT
15:00 CDT
(c)Base and the perturbed PBLH (m) for Sep 9, 2023
9:00 CDT
12:00 CDT
15:00 CDT
PBLH (m)
2500
2000
1500
1000
500
0

Figure 7 Spatial variation in PBLH (m) from [Base], [PBLH5], [PBLH12], and [PBLH14] over the land, the Bay, and Gulf for September 9, (a) 2021, (b) 2022, and (c) 2023. Dot overlaid on the map is the ceilometer observed PBL from the LaPorte, University of Houston Pontoon Boat (UHPB), Red Eagle boat (RE), MAQL1, MAQL2, and Osprey Boat (OB).

In September 2022, the base simulation shows very low PBLH during noon and the afternoon over the water, which contrasts with the ceilometer-observed PBLH. The perturbed simulations in this case show an increase in PBLH over the water which is more comparable to the observed PBLH. The increase in PBLH is more pronounced in PBLH12 and PBLH14 where the NSAS cumulus scheme is used, compared to PBLH5 where the cumulus scheme is the same as in the base, but the closure constant value is perturbed. In September 2023, the base simulation shows a very low PBLH even over the land across the selected hours. For example, in the morning at 9:00 CDT, the base model along with all the three perturbation simulations underestimates the PBLH compared to the observation. During the noon, the base simulation still shows a very low PBLH across the region, while PBLH12 and PBLH14 show higher PBLH over the land compared to the base, getting closer to the observation. PBLH5 shows only a slight increase in PBLH compared to the base.

In summary, PBLH5 and PBH12 show an increase in PBLH during the daytime, getting closer to the observation in 2021, over the Bay. For this period and the region, PBLH14 only increases the PBLH till noon. In 2022, over the Bay all three perturbation simulations show an increase in PBLH compared to base simulation till noon, improving the prediction. However, all three simulations do not show much effect in the afternoon. However, the cloud-like artifact present in the base simulation are resolved in the PBLH12 and PBLH14 in all predictions. The observations for 2023 are similar to in 2022.

To further understand the effects of perturbation simulation on the PBLH over the land and water, we separated the land and water PBLH data and compared it with the HSRL-2 datasets. HSRL-2 covers most of the urban Houston, the Bay, and Gulf regions for September 2021. Here in this analysis, we selected 7 days of high ozone days in September 2021 for the comparison. **Figure 8** presents the diurnal variation boxplots for September 8-9 and September 23-27, 2021, for the selected best perturbation simulations (PBLH5, PBLH12, PBLH14), the base model, and HSRL-2 over the land and water. The diurnal variation of PBLH is more prominent over land compared to water. Over land (**Figure 8a**), between 10:00-13:00 CDT, PBLH14 is the most similar to the HSRL-2 among all four WRF simulations (Base, PBLH5, PBLH12, and PBLH14). The Base, PBLH12, and PBLH5 models overestimated the PBLH by ~200 m. From 14:00-17:00 CDT, the base, PBLH5, and PBLH12 simulations performed better, while PBLH14 slightly underestimated the PBLH. PBLH14 is the simulation with the implementation of UCM which results in a decrease in PBLH over the land in the afternoon compared to the base.

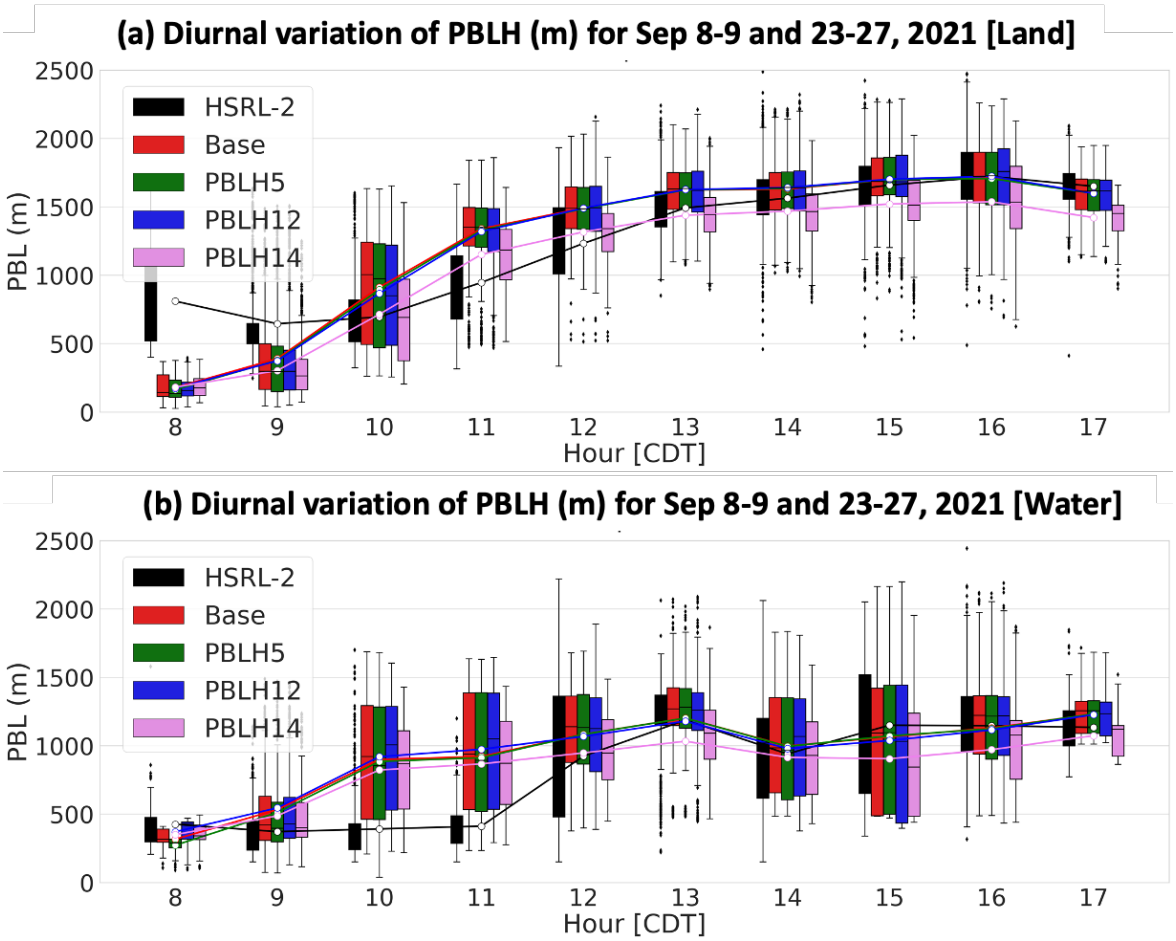

Figure 8 Boxplot of the diurnal variation of PBLH over the (a) Land and (b) Water for September 8-9 and 23-27, 2021. Color in the boxplot represent the PBLH from HSRL-2 (Black), Base (Red), PBLH5 (Green), PBLH12 (Blue), and PBLH14 (Violet)

Figure 8b compares the diurnal variation of PBLH for selected days in September 2021 over water. In the morning, all models overestimate the PBLH by an average of 300 m compared to the HSRL-2 which shows a relatively low PBLH (~500 m). This is consistent with the frequency distribution plot of boat-based PBLH observations (Figure 4a) where all the simulations overestimated the PBLH in the morning (i.e., the first peak in frequency). PBLH14 aligns more closely with the observations in the morning. After 12:00 CDT, the base, PBLH5, and PBLH15 are more aligned with the observations, whereas PBLH14 slightly underestimates the PBLH. The boxplot shows that the model PBLH varies widely in the morning, with a range from 400 to 1200 m, while HSRL-2 shows less variability. In the afternoon, all models and the HSRL-2 show higher variability, for example at 14:00 and 15:00 CDT. Overall, in September 2021, as observed from the upper and lower quantiles, PBLH variability within each hour is higher over water

compared to land. Higher variability observed over the water might be due to the differences between the Bay and the Gulf as shown in the ceilometer-based PBLH observations. The limited HSRL-2 data over the waters does not allow for a statistically meaningful delineation of PBLH between the two water bodies.

4.4. Effect of model perturbations on meteorology

This section presents the effects of the perturbation simulations on the meteorological variables for the selected days described in Section 3.3, namely: July 27-28 and September 9, 2021; September 8-10, 2022; and May 19 and September 9-10, 2023, over the Bay and the Gulf. **Figure 9** shows the spatial variability of temperature compared to the base simulation, along with the differences between the perturbed and base simulations for the three selected perturbation simulations (PBLH5, PBLH12, and PBLH14). Over the Bay, the base simulation temperature closely follows the observed values, with a slight overestimation of ~0.5-1°C in and around the HSC. Compared to the base simulation, all three selected perturbation simulations show a temperature decrease (~0.5-1°C) around the HSC, suggesting that the perturbation simulations slightly improve temperature prediction over the HSC. For other regions of the Bay, the base simulation slightly overestimated the temperature by ~0.5°C in 2021, and the PBLH5 is better in simulating temperature compared to PBLH12 and PBLH14. In 2022, all the perturbation simulations performed better than the base compared to the observed temperature. Over the Gulf, for the selected days, the base simulation underestimated the temperature by ~1°C. Compared to the base simulation, in the northeastern part of the Gulf, PBLH14 and PBLH5 show an increase in temperature, getting closer to the observations. But in the southern part of the Gulf, the perturbation simulations show little change in temperature compared to the base. Overall, around the HSC region all three perturbation simulations perform better compared to base simulation. PBLH14 performs better over the eastern part of the Bay and PBLH5 performs better over the Gulf.

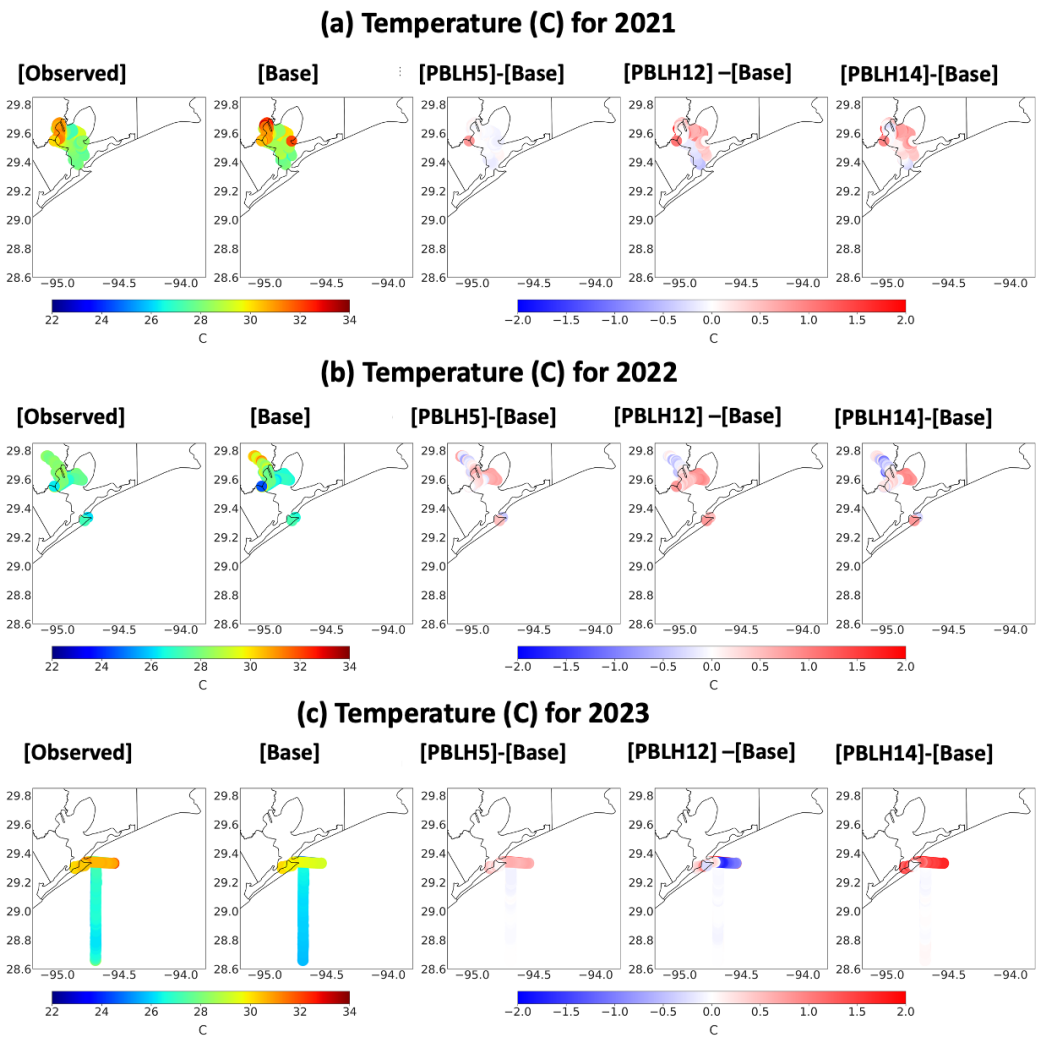

Figure 9 Spatial variation of observed, WRF [Base], [PBLH5] minus [Base], PBLH12 minus [Base], and PBLH14 minus [Base] Temperature (C) for the selected days (a) July 27-28 and September 09, 2021, (b) September 8-10, 2022, and (c) September 9-10, 2023, for the Bay.

Figure 10 shows the spatial variability of wind speed compared to the base simulation, along with the differences between the base and the three selected perturbation simulations (PBLH5, PBLH12, and PBLH14). For the selected simulation days, the base simulation generally overestimated wind speed compared to the observations. In 2021, the base simulation overestimated the wind speed by approximately 1.5-2 m/s. All three perturbation simulations show a decrease in wind speed compared to the base, with a larger decrease (~1 m/s) in PBLH12 and PBLH14, and a smaller decrease in PBLH5. Around the eastern part of the Bay, the base simulation underestimates the wind speed, while the perturbed PBLH12 and PBLH14

simulations show an increase in wind speed (~2 m/s) compared to the base. In 2022, the base simulation underestimates the wind speed by ~1 m/s compared to the observations. All the perturbed simulations show an increase in wind speed in 2022 compared to the base, getting closer to the observations, with PBLH5 performing better than PBLH12 and PBLH14. In 2023, the base simulation overestimates wind speed in the southern Gulf by approximately 2-3 m/s compared to the observations and slightly underestimates it around the northeastern part of the Gulf. Compared to the base simulation, in the southern Gulf, PBLH12 and PBLH14 show a decrease in wind speed (~0.5 m/s), while around the northeastern part, they show an increase in wind speed (~2 m/s). PBLH5 performs better in predicting wind speed over the northeastern part of the Gulf compared to PBLH12 and PBLH14.

Overall, the base simulation either highly overestimated or underestimated the wind speed over the Bay and Gulf, depending on locations. These overestimations and underestimations in wind speed are mitigated to some extent by the perturbation simulations. Among the three perturbation simulations, wind speed is better estimated by PBLH5 over the northern HSC and northeastern Gulf, while PBLH12 and PBLH14 perform better in other parts of the Bay and Gulf.

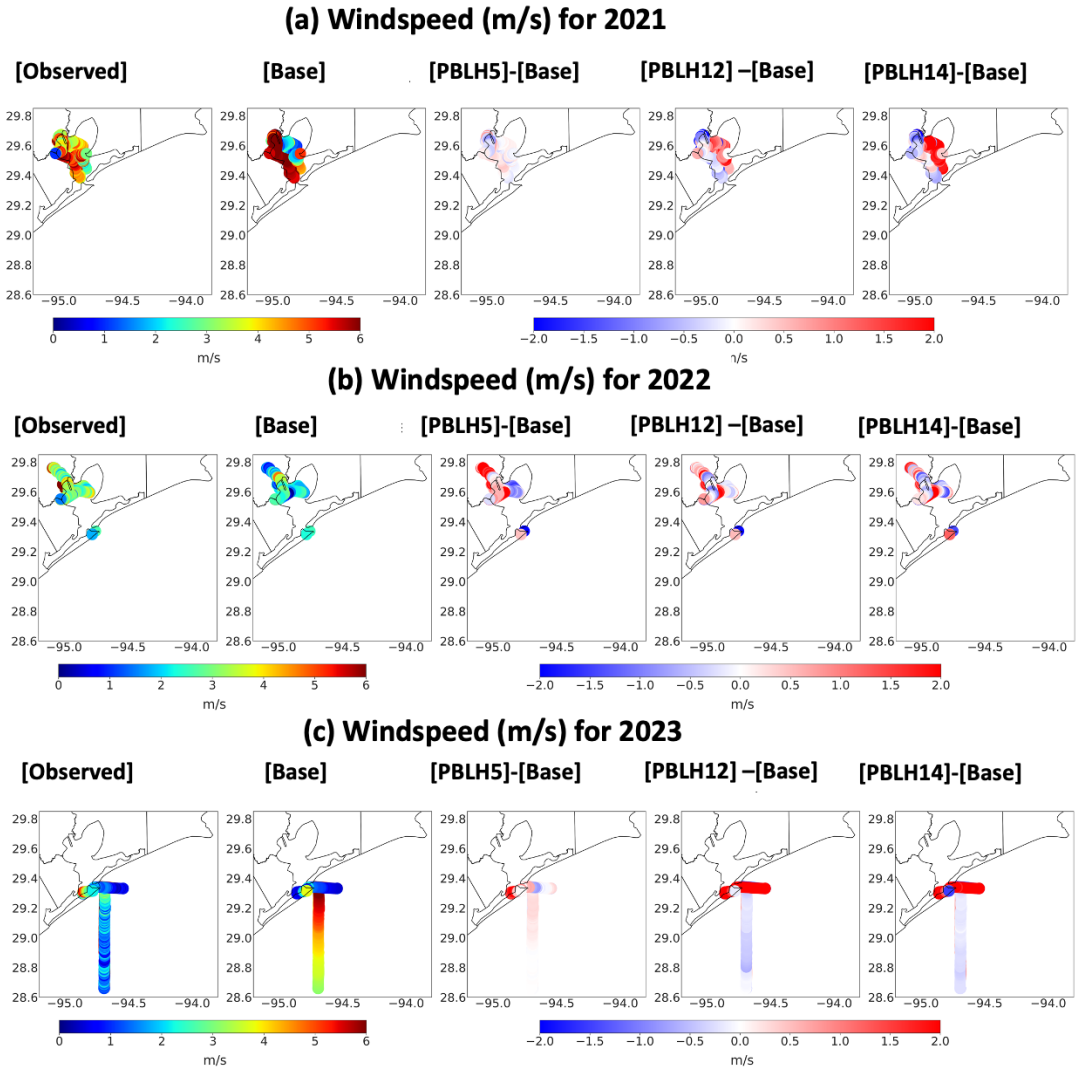

Figure 10 Spatial variation of observed, WRF [Base], [PBLH5] minus [Base], PBLH12 minus [Base], and PBLH14 minus [Base] Windspeed (m/s) for the selected days (a) July 27-28 and September 09, 2021, (b) September 8-10, 2022, and (c) September 9-10, 2023, for the Bay.

5. Conclusion

PBL-related parameterizations in WRF need improvements and tuning to better match observations over water bodies around Houston/Galveston. This task identified key parameters and constants in the MYNN PBL scheme that influence the evolution and development of PBLH over water. Based on the sensitivity of these parameters to PBLH, multiple perturbation simulations were performed to improve the model's performance by fine-tuning the parameters.

In addition to perturbing physical parameters in the model, sensitivity simulations were also conducted by selecting different cloud and urban physics schemes because the base WRF model was found to exhibit unrealistic PBLH features that were traced back to those configurations. A total of 9 days were chosen for model perturbation/sensitivity simulations, with each simulation run for all 9 days, resulting in more than 200 simulation days.

PBLH from different WRF4.6.0 sensitivity simulations were evaluated by comparing with the onshore and offshore observation data from TAQ1, TAQ2, and TAQ3. From various perturbation simulations, we selected three sets of simulations: PBLH5, PBLH12, and PBLH14, which improved the PBLH prediction over the water without considerably affecting performance over the land. PBLH5 refers to perturbed value of closure constant C3. PBLH12 refers to the simulations that implement newer cumulus schemes called NSAS. PBLH14 includes a combination of the UCM with the NSAS cumulus scheme.

By comparing the perturbed PBLH experiments with the base simulation and observations, all three of the selected perturbation simulations provide better PBLH estimates than the base model (by increasing PBLH up to 400 m) when the observed PBLH values are high offshore. When the observed PBLH values are low, mostly over the Gulf, the perturbation simulations show little difference compared to the base model. Overall, over the water in the morning, PBLH14 performed better in predicting the PBLH, while in the afternoon, PBLH12 performed better.

The perturbation simulations show less effect on temperature compared to wind speed. Since the base model captures temperature variability with less bias over the water, the perturbations do not significantly affect the temperature. Among the three perturbations, PBLH14 performs better in temperature prediction over the eastern part of the Bay, while PBLH5 performs better over the Gulf. The base model shows higher biases in wind speed over the Gulf and these biases are reduced by ~1 m/s by the perturbation simulations. Among the three perturbation simulations, wind speed is better estimated by PBLH5 over the northern HSC and northeastern Gulf, while PBLH12 and PBLH14 perform better in other parts of the Bay and Gulf.

The analysis performed in this task presents that WRF model performance in offshore PBL can be improved by fine-tuning the physical parameters of the PBL scheme within the published ranges and by different configurations of the cloud and urban physics schemes. The three selected perturbation models all improve upon the base model in predicting offshore PBL and meteorology, although the specific best perturbations are dependent on the time of day and region. In the subsequent work of the project, we will continue the investigation of the perturbation experiments concerning their abilities to simulate the residual layer (Task 5). The final task of the project (Task 6) will examine the impacts of those perturbation experiments on photochemistry. During those tasks, we will be open for additional parameters and physics

configurations for better simulation of the residual layer, photochemistry, and other aspects of the model.

6. References:

Chen, F., & Dudhia, J. (2001). Coupling an advanced land surface–hydrology model with the Penn State–NCAR MM5 modeling system. Part I: Model implementation and sensitivity. *Monthly Weather Review*, *129*(4), 569–585.

Chen, F., Janjić, Z., & Mitchell, K. (1997). Impact of atmospheric surface-layer parameterizations in the new land-surface scheme of the NCEP mesoscale Eta model. *Boundary-Layer Meteorology*, *85*(3), 391–421.

Huang, Y., & Peng, X. (2017). Improvement of the Mellor–Yamada–Nakanishi–Niino Planetary Boundary-Layer Scheme Based on Observational Data in China. *Boundary-Layer Meteorology*, *162*(1). https://doi.org/10.1007/s10546-016-0187-0

Iacono, M. J., Delamere, J. S., Mlawer, E. J., Shephard, M. W., Clough, S. A., & Collins, W. D. (2008). Radiative forcing by long-lived greenhouse gases: Calculations with the AER radiative transfer models. *Journal of Geophysical Research: Atmospheres*, *113*(D13).

Jensen, M. P., Flynn, J. H., Judd, L. M., Kollias, P., Kuang, C., McFarquhar, G., Nadkarni, R., Powers, H., & Sullivan, J. (2021). A Succession of Cloud, Precipitation, Aerosol, and Air Quality Field Experiments in the Coastal Urban Environment. *Bulletin of the American Meteorological Society*, *102*(2). https://doi.org/10.1175/BAMS-D-21-0104.1

Liu, L., Menenti, M., & Ma, Y. (2022). Evaluation of Albedo Schemes in WRF Coupled with Noah-MP on the Parlung No. 4 Glacier. *Remote Sensing*, *14*(16). https://doi.org/10.3390/rs14163934

Liu, X., Wang, Y., Wasti, S., Li, W., Soleimanian, E., Flynn, J., Griggs, T., Alvarez, S., Sullivan, J. T., Roots, M., Twigg, L., Gronoff, G., Berkoff, T., Walter, P., Estes, M., Hair, J. W., Shingler, T., Scarino, A. J., Fenn, M., & Judd, L. (2023). Evaluating WRF-GC v2.0 predictions of boundary layer height and vertical ozone profile during the 2021 TRACER-AQ campaign in Houston, Texas. *Geoscientific Model Development*, *16*(18). https://doi.org/10.5194/gmd-16-5493-2023

Morrison, H., Thompson, G., & Tatarskii, V. (2009). Impact of cloud microphysics on the development of trailing stratiform precipitation in a simulated squall line: Comparison of one-and two-moment schemes. *Monthly Weather Review*, *137*(3), 991–1007.

Nakanishi, M., & Niino, H. (2009a). Development of an improved turbulence closure model for the atmospheric boundary layer. *Journal of the Meteorological Society of Japan. Ser. II*, *87*(5), 895–912.

Nakanishi, M., & Niino, H. (2009b). Development of an improved turbulence closure model for the atmospheric boundary layer. *Journal of the Meteorological Society of Japan*, *87*(5). https://doi.org/10.2151/jmsj.87.895

Pithan, F., Angevine, W., & Mauritsen, T. (2015). Improving a global model from the boundary layer: Total turbulent energy and the neutral limit Prandtl number. *Journal of Advances in Modeling Earth Systems*, *7*(2). https://doi.org/10.1002/2014MS000382

Tiedtke, M. (1989). A comprehensive mass flux scheme for cumulus parameterization in large-scale models. *Monthly Weather Review*, *117*(8), 1779–1800.

Yang, B., Qian, Y., Berg, L. K., Ma, P. L., Wharton, S., Bulaevskaya, V., Yan, H., Hou, Z., & Shaw, W. J. (2017). Sensitivity of Turbine-Height Wind Speeds to Parameters in Planetary Boundary-Layer and Surface-Layer Schemes in the Weather Research and Forecasting Model. *Boundary-Layer Meteorology*, *162*(1). https://doi.org/10.1007/s10546-016-0185-2

Zhang, C., Wang, Y., & Hamilton, K. (2011). Improved representation of boundary layer clouds over the southeast Pacific in ARW-WRF using a modified Tiedtke cumulus parameterization scheme. *Monthly Weather Review*, *139*(11), 3489–3513.